UCRL--89286

DE83 016790

TMX-U EXPERIMENTAL RESULTS

T. C. Simonen, S. L. Allen, T. A. Casper, J. F. Clauser, C. A. Clower, F. H. Coensgen, D. L. Correll, W. F. Cummins, C. C. Damm, B. H. Failor, M. Flammer, J. H. Foote, R. K. Goodman, D. P. Grubb, D. N. Hill, E. B. Hooper, R. S. Hornady, A. L. Hunt, W. L. Hsu,* R. A. James,† R. G. Kerr, C. Lasnier,† G. W. Leppelmeier, J. M. Moller, A. W. Molvik, T. J. Nash, W. E. Nexsen, W. L. Pickles, P. Poulsen, B. W. Stallard, J. Taska, W. C. Turner, and T. L. Yu**

Lawrence Livermore National Laboratory, University of California
Livermore, California 94550 U.S.A.

ABSTRACT

This paper describes results from the Tandem Mirror Experiment-Upgrade (TMX-U). Mirror-confined electrons with 30-70 keV mean energy densities of 0.5 to 2.0 x 10^{12} cm^{-3} and average betas of 3 to 5% are produced using electron-cyclotron resonant heating (ECRH). These results are consistent with an electron Fokker-Planck code. Improved ion-cyclotron microstability is observed using neutral beam injection at 47 deg to the magnetic axis, rather than at 90 deg as in the previous experiment, TMX. Strong end plugging has been produced using a combination of ECRH gyrotrons with sloshing-ion beam injection. In these low-density central cell experiments (3 x 10^{11} cm^{-3}) the axial losses ($\tau_{\parallel}$ = 20 to 80 ms) are smaller than the nonambipolar radial losses ($\tau_{\perp}$ = 4 to 8 ms). Plugging has been achieved with a central cell density double that of the end plugs. Although no direct measurements are yet available to determine if a thermal barrier potential dip is generated, these experiments support many theoretical features of the thermal barrier concept.

I. Introduction

The Tandem Mirror Experiment-Upgrade (TMX-U) [1] shown in Fig. 1 was built to investigate the tandem mirror thermal barrier [2] concept. A schematic diagram of the magnet and neutral beam systems are shown in Fig. 2. Thermal

KEY WORDS: tandem mirrors, thermal barrier, magnetic mirrors, TMX-U.

*Sandia National Laboratory, Livermore, CA 94550
**Johns Hopkins University, Baltimore, MD 21218
†University of Maryland, College Park, MD 20742

Figure 1. Photograph of the TMX-U device.

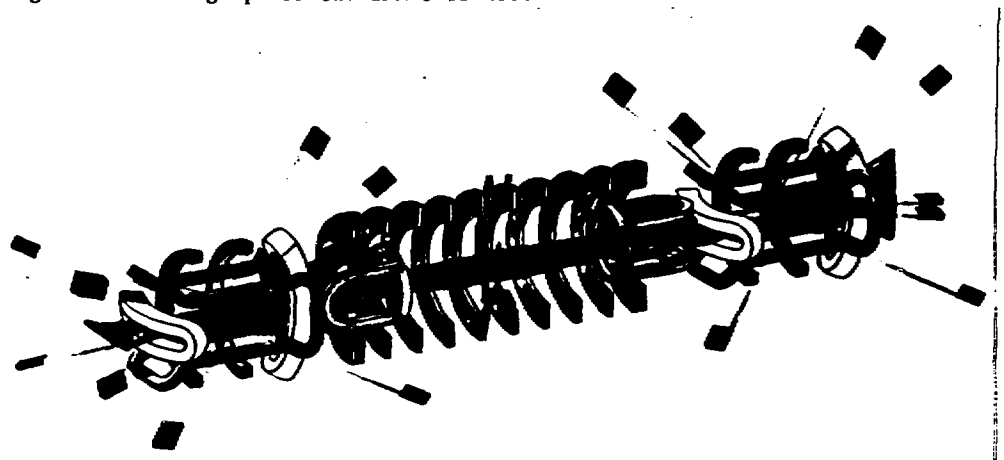

Figure 2. Artist's drawing of TMX-U magnet and neutral beam system.

barriers improve end plug ion microstability and allow the generation of higher electrostatic confining potentials to increase central cell ion confinement.

As indicated in Fig. 3, in the earlier TMX standard tandem experiment [3-5] central cell electrostatic confining potential ϕ_c was generated by a high density end plug [6,7]

$$\phi_c = T_e \ln \frac{n_p}{n_c} \quad , \tag{1}$$

where T_e is the electron temperature and n_p and n_c are the plug and central cell plasma densities. Low energy ions that are required for end plug ion microstability were supplied by leakage of central cell ions. However, when scaling the standard tandem mirror to a reactor, [8] the high end plug densities required to generate high-confining potentials lead to high-field minimum-B magnets and high energy neutral beams. In addition, supplying the low-energy ions for microstability lead to high power drain. These disadvantages are overcome in the thermal barrier tandem mirror.

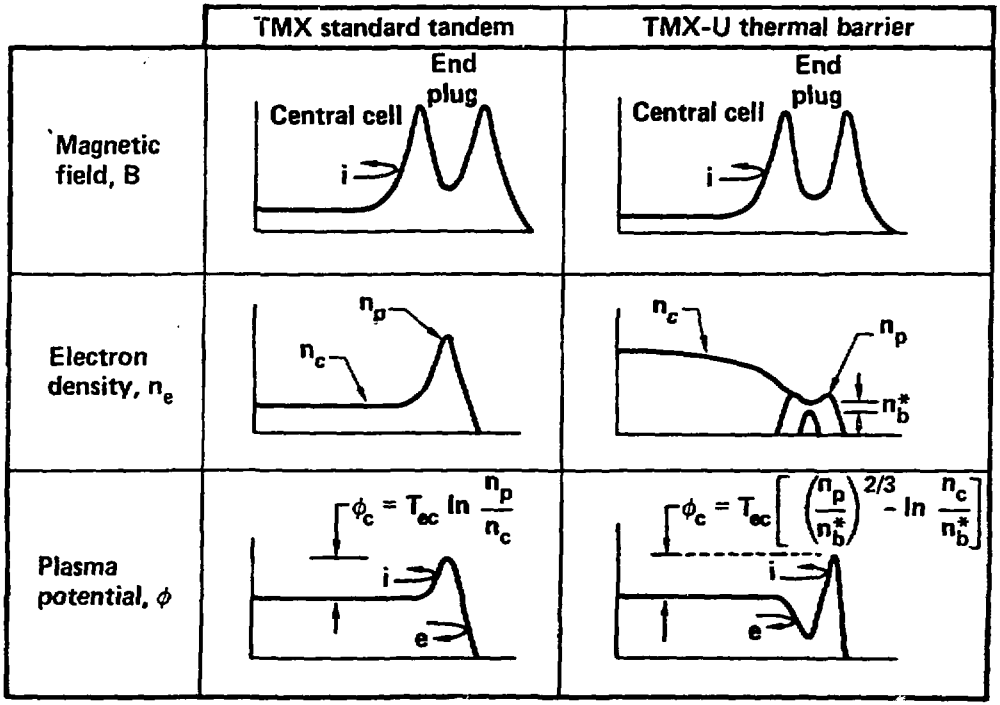

Figure 3. Schematic diagram of tandem mirror axial profiles.

In the thermal barrier concept microwave heating power is used to generate high potentials with low end plug densities. A potential peak off the plug midplane is driven by ECRH and supported by a density peak in magnetically trapped ions--in TMX-U beams are injected at the midplane at 47 deg to the magnetic axis. The potential dip at the end plug midplane reduces the microwave heating power needed to generate the potential peaks at the outside

of each end plug by isolating the electrons in the potential peak from the cooler central cell electrons. Oblique injection, rather than the orthogonal used in TMX, improves the stability of the Alfven ion cyclotron (AIC) mode, which was the main microinstability observed in TMX. [9] The tipped potential allows low-energy central cell ions to be confined within the end plugs for microstability. Thus, these ions do not introduce an extra power drain.

The central cell confining potential depends on the strength of the microwave heating power. If the ECRH power is low, [2]

$$\phi_c = T_{ep} \ln \frac{n_p}{n_b^*} \left(\frac{T_{ec}}{T_{ep}}\right)^{1/2} - T_{ec} \ln \frac{n_c}{n_b^*} , \qquad (2)$$

where n_b^* is the non-mirror-confined electron density at the end cell midplane. Here we see the advantage of having a high fraction of mirror-confined electrons (i.e., making n_b^* small). In this model the plug and central cell electron temperatures (T_{ep} and T_{ec}) are assumed to be Maxwellian. When the ECRH power is high, the electron distribution is strongly distorted from Maxwellian and the resulting confining potential is [10,11]

$$\phi_c/T_{ec} = \left(\frac{3}{4}\sqrt{\pi}\,\frac{R_{pb}^{-1}}{R_{pb}}\,\frac{n_p}{n_b^*}\exp\left\{\phi_b/[T_{ec}(R_{mb}-1)]\right\}\right)^{2/3} - \ln\frac{n_c}{n_b^*} . \qquad (3)$$

Here R_{pb} is the mirror ratio from the potential peak to the barrier, R_{mb} is the mirror ratio of the inner mirror to the barrier, and ϕ_b is the potential drop from the central cell to the barrier minimum. Equation (3), which is derived in Ref. 10, reduces to an approximate form for TMX-U parameters,

$$\phi_c/T_{ec} = \frac{2}{3}\left(\frac{n_p}{n_b^*}\right)^{2/3}\left(\frac{n_c}{n_b^*}\right)^{1/5} - \ln\frac{n_c}{n_b^*} . \qquad (4)$$

The TMX-U experiment operates in the strong radio frequency (rf) limit described by Eq. (4).

The TMX-U machine parameters are given in TABLE I. For comparison we also list those of TMX. TMX-U began subsystem commissioning in early 1982 and began first physics experiments in the summer of 1982.

II. Thermal Barrier Startup

A characteristic of mirror systems is that confinement improves at high temperatures. The consequence of this favorable behavior means that the temperature must be raised at low density and then the density increased. Alternatively, high-power startup heating systems could be employed to reach equilibrium confinement conditions.

In TMX-U we are following the low density startup approach outlined in Fig. 4 and TABLE II. This figure shows the axial profiles of magnetic field, density, and potential at each phase in the startup time sequence. First, hot electron density buildup begins at low density to accomodate the ECRH power requirement. When the source plasma electron temperature is low, collisional losses of rf-trapped electrons are reduced if the source density is also low. As the hot electron end plug density builds up above that of the central cell, a small dip in potential must form to hold ions to charge-neutralize the mirror-confined electrons (see Fig. 4).

TABLE I. Comparison of machine parameters for TMX and TMX-U.

System	TMX	TMX-U
Magnet		
End plug midplane field (T)	1.0	0.5
Plug-mirror ratio	2:1	4:1
Plug length (m)	0.9	3.0
Central cell length (m)	5.5	8.0
Central cell field strength (T)	0.2	0.3
Magnet power system (MW)	13	26
Neutral beam		
Injection energy (kV)	20	20
Duration (ms)	25	75
Maximum power (MW)	5	10
Plug injection angles (deg)	90	47,18
Central cell injection angle (deg)	90	70,58.5
Electron-cyclotron resonant heating		
Number of gyrotrons	0	4
Maximum power per gyrotron (kW)	--	200
Frequency (GHz)	--	28
Duration (ms)	--	75
Ion-cyclotron resonant heating		
Power (MW)	0	0.2
Frequency (MHz)	--	2-5
Duration (ms)	--	>100
Vacuum		
Overall machine length (m)	15	22
Volume (m^3)	120	225
Pumping speed (10^6 liters/s)	30	50

Sloshing beam injection is initiated once the hot electron line density is sufficiently high to trap the beams, approximately 10^{13} cm^{-2}. The sloshing-ion density then builds up as in step 2 provided the cold gas density is sufficiently low compared to the sloshing beam atom density. Positive peaks must now develop to confine the electrons necessary to charge-neutralize the magnetically confined ions. Simultaneously the potential profile adjusts as in step 3 because the ECRH power boils electrons out of the outer potential peak.

The fourth and final step, not shown on Fig. 4, is to increase the density while maintaining the high temperature. The requirements outlined for this step in TABLE II suggest that ICRH can help [12] increase the central cell ion temperature T_{ic} at low density and that pump beams can help the sloshing beams pump out the thermal barrier. Once the central cell line density is sufficient (about 10^{14} cm^{-2}), neutral beam heating can augment ICRH and become the dominant source of central cell heating.

At present, the TMX-U experiments have progressed to step 3 and are beginning step 4. In the remaining sections of this report we describe our results during each of these startup phases.

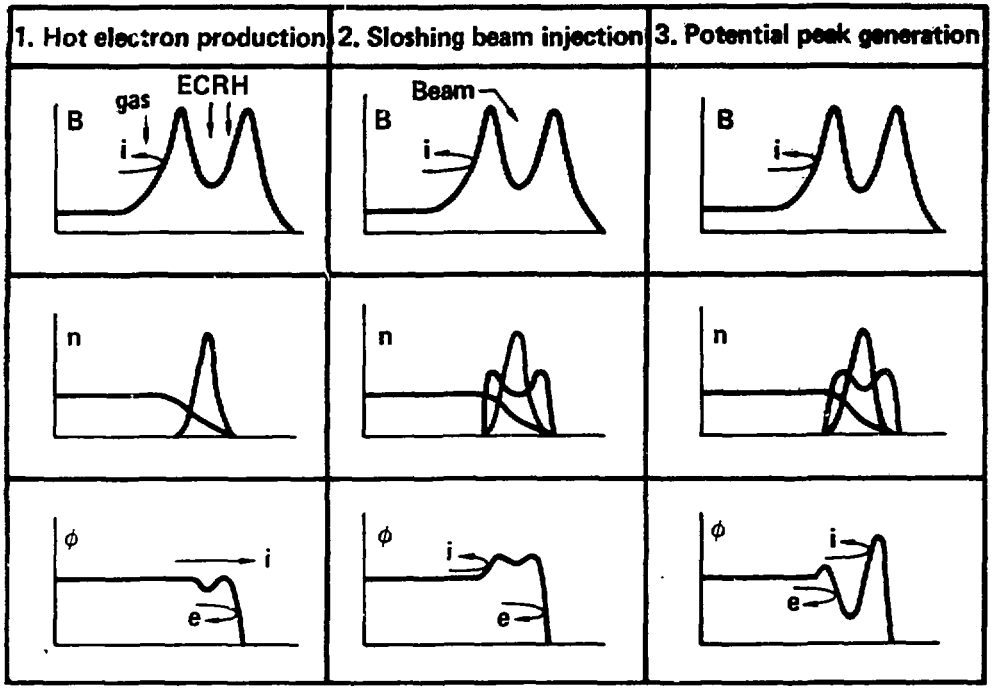

Figure 4. Schematic diagram of TMX-U thermal barrier startup sequence.

TABLE II. Thermal barrier startup sequence. The equipment and requirements of each preceeding step are necessary for each subsequent step.

Step	Equipment	Requirements
1. Hot electron production	ECRH, Gas feed	Low n_{ec} for efficient rf trapping
2. Sloshing beam injection	Sloshing beams	$n_{gas} < n_{beam}$
3. Potential formation	As in 1 and 2	As in 1 and 2
4. High density buildup	Central cell gas puffing, Central cell ICRH, 18 deg pump beams, Central cell beams.	Barrier filling $\propto n_{ic}^2/T_{ic}^{3/2}$ $\int n_c dl > 10^{14}$ cm^{-2}

III. Hot Electron ECRH Experiments

Hot electron experiments [13] are carried out using ECRH and central cell gas feed. Power from separate 28-GHz microwave gyrotrons is beamed to the 0.5- and 1.0-T end plug locations indicated in Fig. 4. The time history of the power incident on the plasma from each gyrotron is shown in Fig. 5. The

diamagnetic loop measures the energy stored in the magnetically confined hot electrons. Figure 5 shows that the time derivative of stored energy triples when the second gyrotron is turned on; this indicates that the efficiency of hot-electron heating with both gyrotrons is greater than with the fundamental only. Two axially offset diamagnetic loops determine that the hot electron total length, L_{eh}, is approximately 120 cm. The hot-electron Gaussian radius is estimated to be 13 cm from skimmer probe experiments on another day. From Fig. 5 we can determine that the hot electron energy content reaches $W \approx 10^{-8}_{m}\, BL_{eh} \approx 10^{-8}$ (60 to 90) x kA cm^2/cm x 5 x 10^3 G x 120 cm ≈ 360 to 540 J. Here B is the midplane magnetic field strength. From the rate of rise of diamagnetic signal, 13 to 20 J/ms, we determine a 15 to 22% efficiency for conversion of ECRH power to magnetically trapped electrons. From Fig. 5, the hot electron loss power can be estimated from the 20 ms diamagnetic loop decay time constant after ECRH turnoff; 360 to 540 J/20 ms ≈ 18 to 27 kW. Additional ECRH power is consummed in gas ionization and in heating the untrapped plasma stream as indicated in TABLE III. We can account for one-half to two-thirds of the power that leaves the ECRH horns. Since the gas feed effects n_{ec} and T_{ec}, we expect there is an optimum central cell gas-feed current for nearly constant values of rf power and pulse

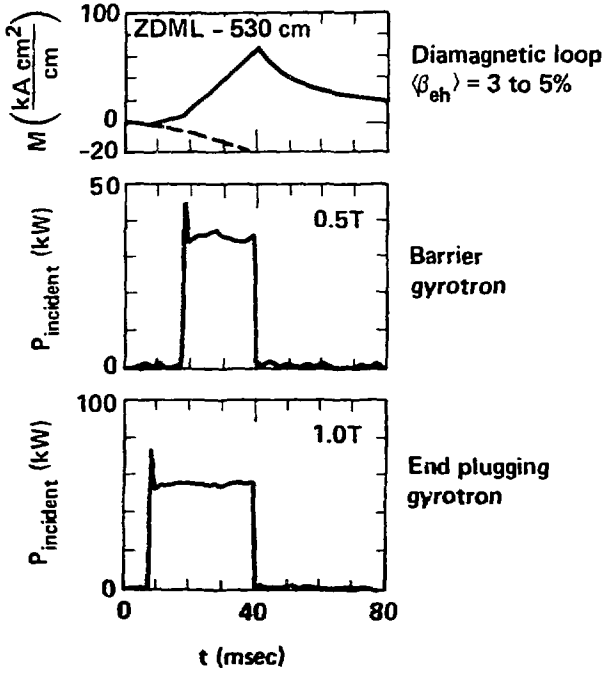

Figure 5. Time history of the hot-electron diamagnetic signal. This shot produced one of the highest TMX-U diamagnetic signals. Note that buildup is limited by the gyrotron duration. The uncertainty in the baseline is caused by variations in the magnet currents.

TABLE III. Estimate of power balance for the west end plug data of Fig. 5.

Power incident on plasma (kW)	
0.5 T gyrotron	35
1.0 T gyrotron	55
Total	90
Accountable power losses	
Storage in hot electrons (kW)	15 to 22
Hot electron losses (kW)	18 to 27
Gas ionization (200 A x 30 V)	3 to 6
Cold plasma end loss power (7 A x 1 kV)	4 to 7
Total (kW)	40 to 62

length. The peak diamagnetism, shown in Fig. 6, occurs at a gas current of ~2 Torr-liters/s (~22 A). A maximum in the curve is expected. At a high gas current the electron trapping efficiency is low because of a high collision rate (high electron density and low electron temperature). At too low a gas feed the trapping efficiency is higher but buildup is limited by the available particle current.

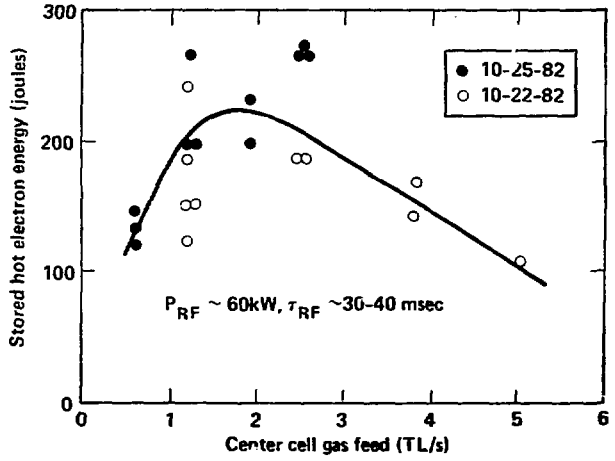

Figure 6. Variation of hot-electron diamagnetism with central cell gas feed shows an optimum.

As Fig. 7 shows the average hot electron beta increases as we progressively increase ECRH power P and pulse length Δt. Depending on the shape of the radial profiles, which are not well known, we have achieved a 3 to 5% volume average beta (half the peak value on-axis). Future operation with a new oversize waveguide system and longer pulse duration gyrotrons should allow 15% volume average betas to be achieved.

Using microwave interferometer density measurements we determine that the average electron energy for the diamagnetism data of Fig. 5 is 48 keV. During

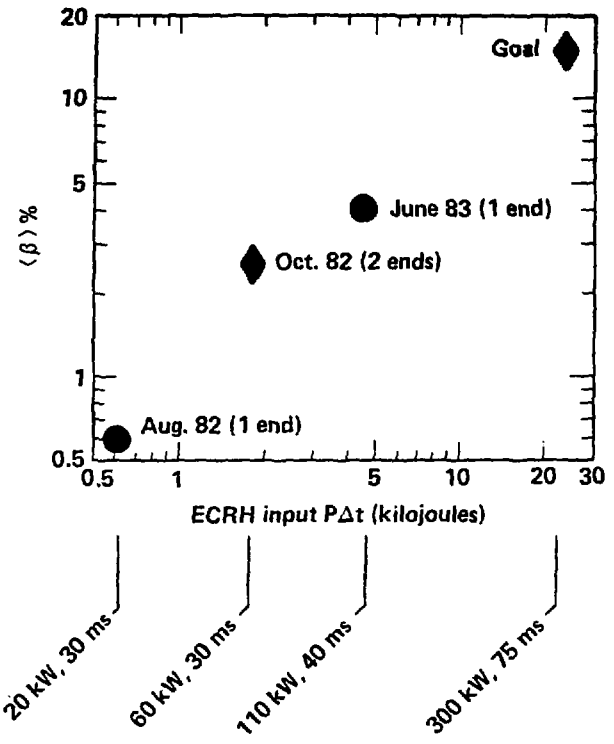

Figure 7. The average hot electron beta increases with incident ECRH power and pulse length.

operation over a wide range of conditions diamagnetic loop and microwave interferometer measurements indicate average electron energies in the desired 30 to 70 keV range.

We can estimate the hot electron coulomb mirror confinement time to be

$$\tau = 0.35\ \tau_{ee} \log R \quad ,$$

where the factor 0.35 accounts for scattering of both electrons and ions and R is the mirror ratio (R = 4 in TMX-U). The 90 deg Coulomb scattering time is $\tau_{ee} = 5 \times 10^8\ T_e^{3/2}/n_e$. For the TMX-U parameters R = 4, 3/2 T_{eh} = 48 keV, and $n_e = 1 \times 10^{12}$ cm^{-3} we calculate τ = 20 ms. This time is the same as estimated from the diagmagnetic loop decay rate.

A central issue concerning hot, mirror-confined electrons is microstability. Whistler and upper-hybrid loss-cone instabilities are predicted to be convectively unstable. [14,15] Using microwave receivers, the University of Maryland group [16] has observed cyclotron emissions enhanced over thermal levels. In some cases these microinstabilities limit the density, the energy buildup, or both. In other cases, such as that shown in Fig. 5, the hot electron beta is limited only by ECRH duration. Figure 8 charts theoretical convective growth length curves for both these electron microinstabilities. As can be seen, while shorter convective growth lengths are predicted as the

density increases, we have not yet encountered any basic limitation caused by hot electron instabilities.

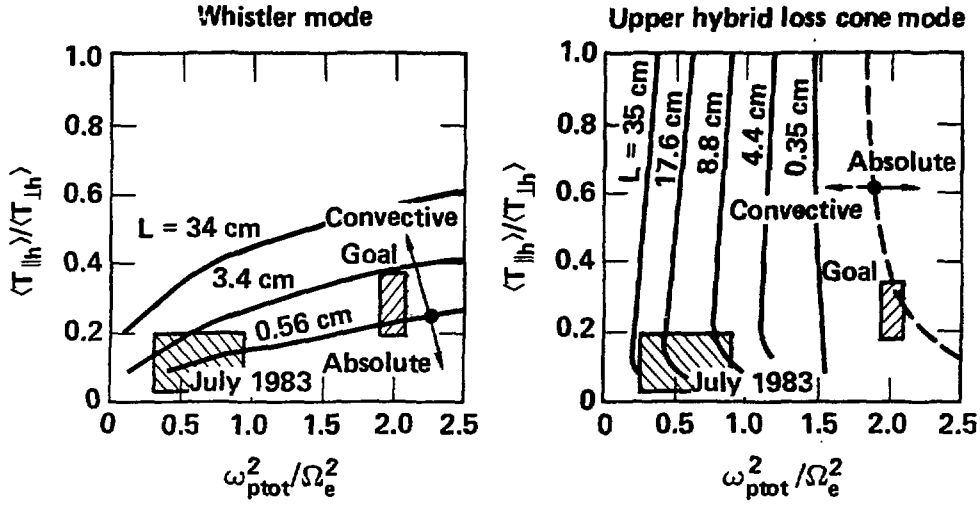

- TMX-U operates at convective-absolute hot electron stability boundary

Figure 8. Constant convective growth length curves for (a) the whistler instability and (b) the upper hybrid loss cone instability (UHLC). In both cases T_h = 40 keV, T_c = 3 keV, and B = 0.5 T. These calculations are for the most unstable UHLC density ratio, n_{eh}/n = 0.6.

In Fig. 9 we compare our experimental results with predictions of the electron Fokker Planck code. [11] Results of the time-dependent code overlap but lie slightly higher than the experimental data. While uncertainties are present in both the experimental data and the code model, we conclude that anomalous loss of hot electrons does not play a dominant role in these TMX-U experiments.

IV. Hot Ion Experiments With Sloshing and Pump Neutral Beams

The first series of TMX-U experiments [17] were carried out with sloshing beam injection, without hot electrons, using ECRH only for preionization and target plasma production. These experiments allowed us to demonstrate that sloshing ions can remain peaked near the injection angle, thereby producing a perpendicular pressure peaked off the plug midplane (see Fig. 10). When charge-exchange of cold gas is included in the Fokker Planck code, good agreement is found between the code and the measured density and charge-exchange spectrum near the injection angle, although the measured signal near 90 deg is higher than predicted. Whether or not this 90-deg signal is caused by charge-exchange or other phenomena needs to be investigated in future experiments.

By inverting the angular distribution we can obtain the axial sloshing ion density profile. [18] Results are shown in Fig. 11. The density dip at the midplane should generate a potential dip which will hold low-energy ions and aid ion cyclotron microstability.

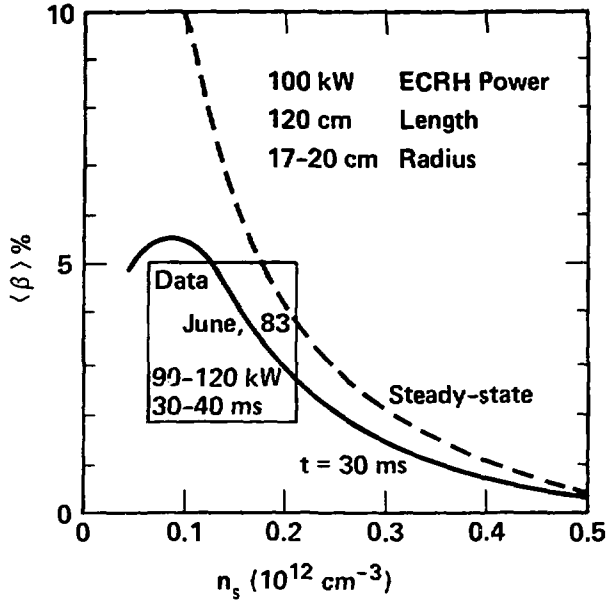

Fig. 9. Comparison of TMX-U hot-electron results with electron Fokker-Planck code results. The average hot-electron beta is seen to depend on the electron density passing into the end plug. During the startup phase n_s is the central cell density. Once a thermal barrier is formed, n_s is the passing electron density and is much less than the central cell density.

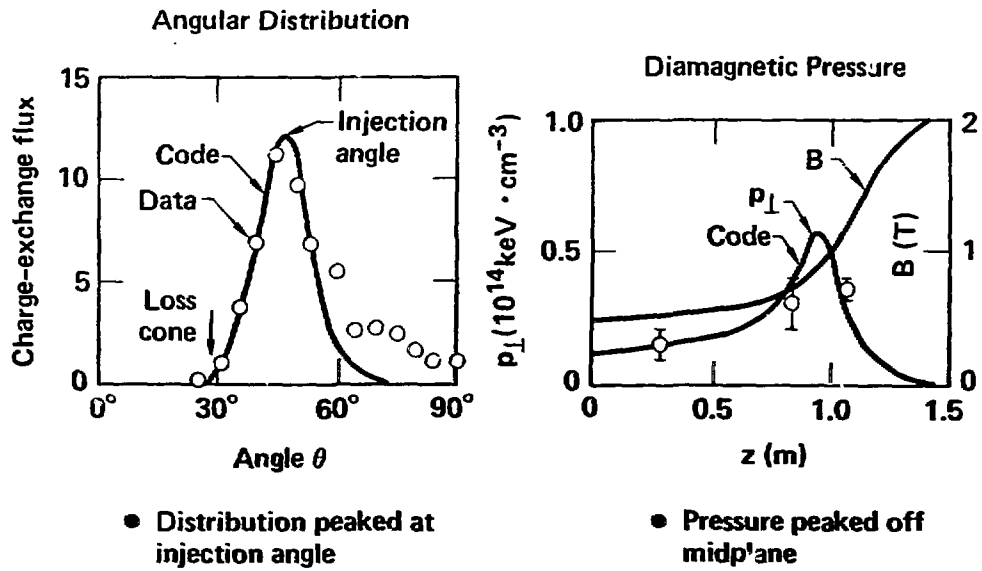

Figure 10. Measurements of the charge-exchange angular distribution and diamagnetic axial distribution are described by an ion Fokker-Planck code.

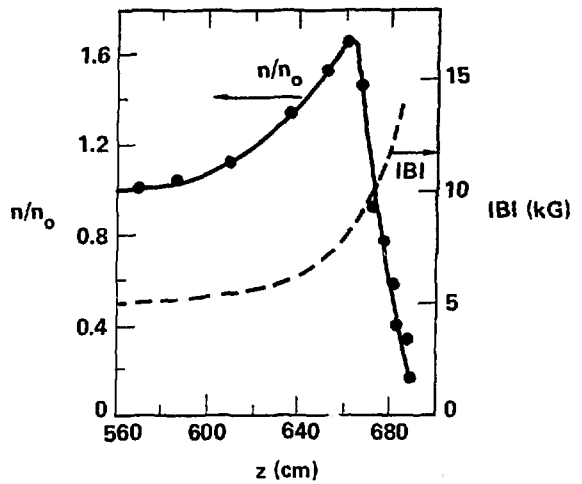

Figure 11. Sloshing-ion axial density profile calculated from charge-exchange angular distribution.

The ion cyclotron fluctuation level in these experiments was low at 5×10^{12} cm^{-3} density, the maximum expected operating density. A comparison of microstability parameters and fluctuation characteristics is given in TABLE IV. The microstability scale length parameters are such that TMX-U is more prone to loss-cone ion-cyclotron instability than TMX was. A very significant result is that for the first time in a neutral-beam-driven mirror machine we have not detected ion cyclotron fluctuations at the midplane ion cyclotron frequency. We attribute this stability to the oblique injection that stabilizes the AIC mode, to the density dip which holds low-energy ions, and to the large end loss flowing through the end plug. In later, lower density experiments described in Section V, microstability is observed without large end losses.

Another measure of the effect of fluctuations on the ions is obtained by measuring the energy spectra of central cell ions escaping out the end plugs. Figure 12 shows that at equal end plug potentials (equal ambipolar loss cone in the end plugs) the central cell ions escaping out of TMX-U are not heated by the ion cyclotron fluctuations, as was the case in TMX.

An important feature of thermal barrier operation is that low-energy ions need to be pumped out of the potential depression. In TMX-U the sloshing beams are aimed at the midplane to charge-exchange away low-energy ions. To augment this process, and to limit the sloshing-ion density to below ECRH cutoff, TMX-U is equipped with pump beams at 18 deg with respect to the magnetic axis (see Fig. 2). Figure 13 demonstrates this charge-exchange pumping technique. Since pump beam ions are in the loss cone, they are not mirror-confined, and they have sufficient energy so that they are not potentially confined. Figure 13 shows that the density, plasma diamagnetism and sloshing-ion density indeed are reduced. The smaller change in total density indicates that the filling rate of low-energy ions is more rapid than the pump-out rate. The pump-out time constant is consistant with the predicted value.

TABLE IV. Comparison of end plug ion microinstability parameters and fluctuation characteristics for TMX and TMX-U. A check (✓) means the issue has been explained by theory, and a question (?) means it has not been addressed by theory.

	TMX	TMX-U	Theoretical Status
Microstability parameters			
Plasma radius in ion gyroradii, r_p/a_i	5	4	
Plasma length in ion gyroradii, L_p/a_i	10	25	
End plug fluctuation characteristics			
Maximum amplitude (V at 2 r_p)	5	1	?
Mode	AIC	Loss cone	✓
Frequency (ω/ω_{cio})	0.85	1.9	✓
Bandwidth ($\Delta\omega/\omega$)	<0.02	<0.1	?
Wavelength ($k_l a_{io}$)	0.3	7	✓
Phase velocity (diamagnetic direction)	Electron	Ion	✓
Bursting	Yes	No	?
Propagation to central cell	Yes	No	✓

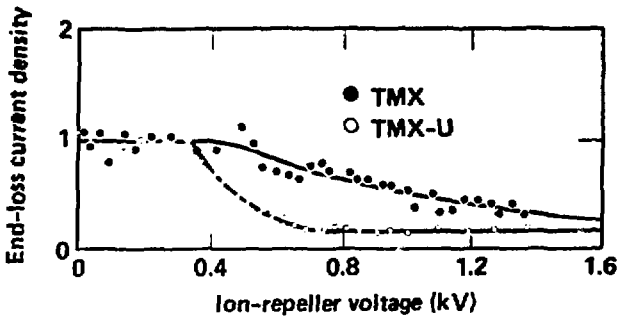

	$3/2\ T_{ic}$ (eV)	$\bar{E}_{end\text{-}wall}$ (eV)
TMX	75	810
TMX-U	100	110

Figure 12. End loss energy spectra at equal potentials show that negligible rf heating of central cell end loss ions occurs in TMX-U. In contrast, instability heating did occur in the previous TMX experiment.

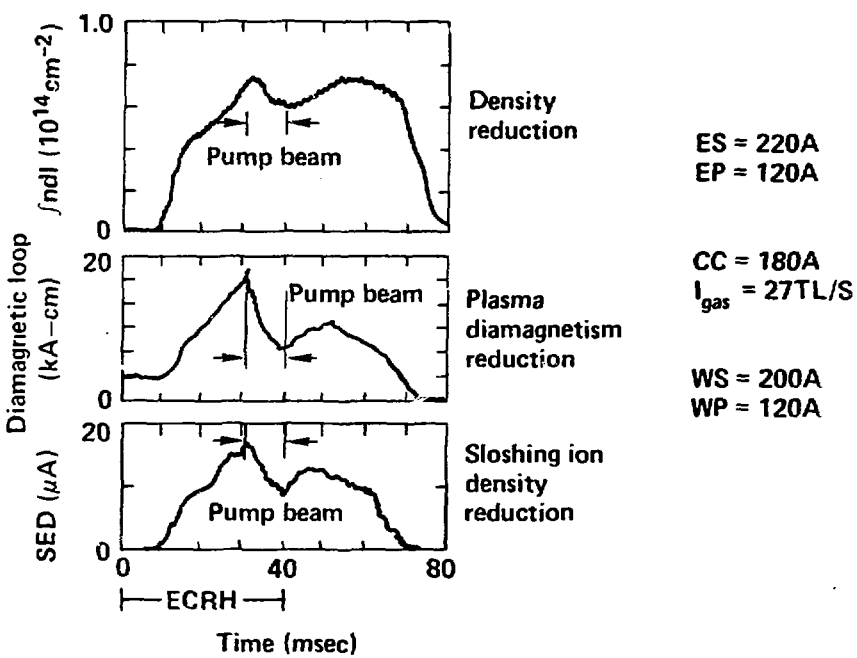

Figure 13. Demonstration of charge-exchange pumping technique. Shown vs time is the (a) line density, (b) diamagnetic loop and, (c) the sloshing ion density. When the pump beam is on the density is reduced.

V. End Plugging Experiments

When the ECRH-produced hot electrons and beam-injected sloshing ions are combined we observe strong end plugging. Results are shown in Fig. 14; they show very low end losses (14e) during the period when both ECRH (14a) and sloshing beams (14b) are operational. Also notice that, in this case, for single-ended operation the end plug density is higher than that of the central cell.

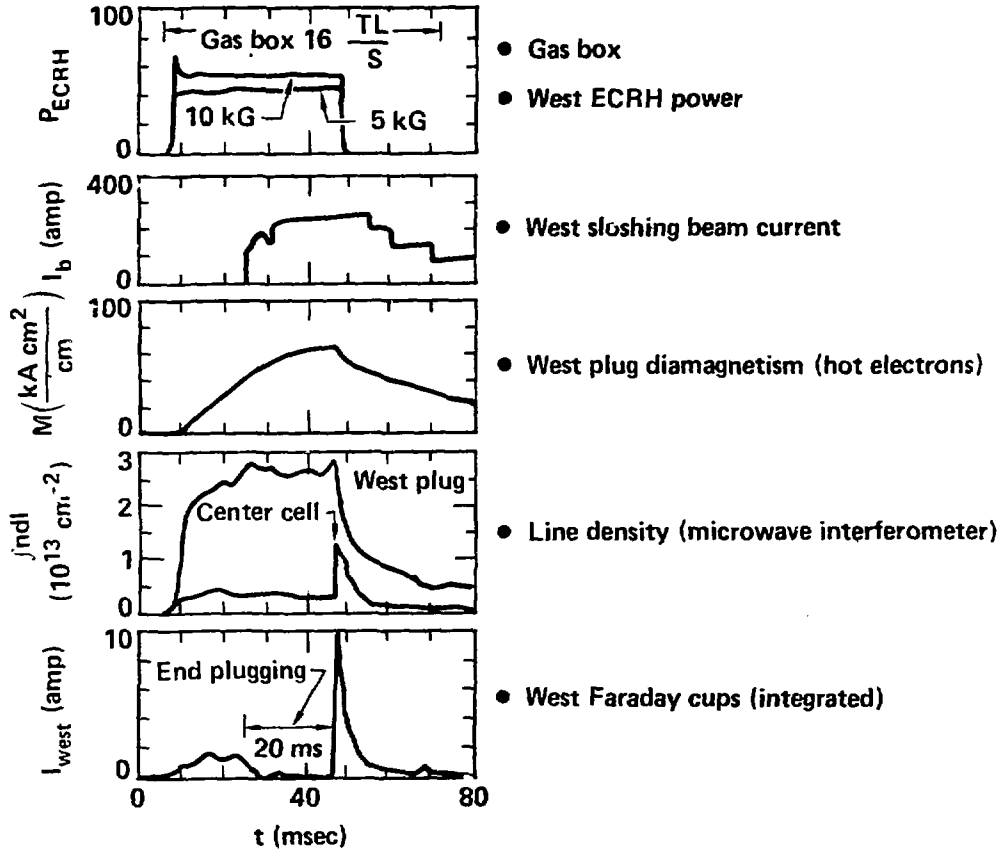

Figure 14. Demonstration of ECRH end plugging. Shown vs time is (a) ECRH power, (b) sloshing beam current, (c) hot-electron diamagnetism, (d) west plug and central cell microwave interferometer line density and, (e) west Faraday cup integrated ion end loss current.

That the end plugging requires sloshing ions is shown in Fig. 15. The injected sloshing beam current is modulated, and the end losses are similarly modulated. On closer examination we find stoppering begins 0.3 ms after sloshing-beam injection. This is the time required to accumulate a density of sloshing ions comparable to the central cell density. When the sloshing beams are turned off, the end losses increase on a 2-ms time scale, characteristic of the sloshing-ion lifetime.

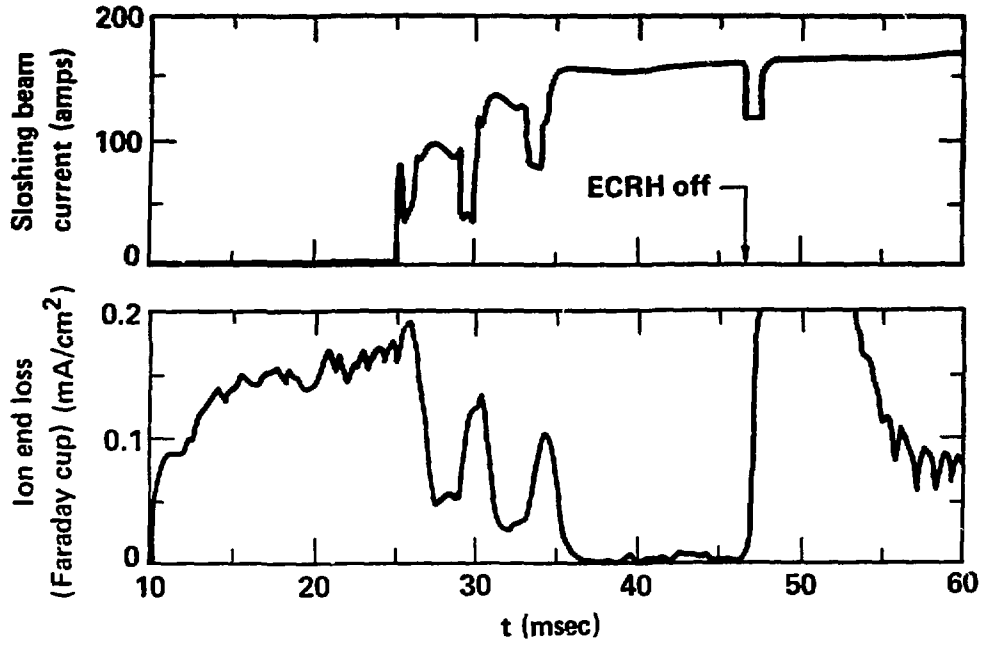

Figure 15. The ion end loss current density, shown vs time, is reduced when sloshing beam current is turned on, demonstrating that end plugging requires sloshing beams.

There are two ECRH gyrotrons illuminating each end plug. The barrier ECRH gyrotron at 0.5 T primarily generates mirror confined electrons with a 20 to 40 ms lifetime (see Fig. 14). The end plugging gyrotron at 1.0 T generates the plugging potential and also produces warm electrons to feed the second-harmonic barrier ECRH. As shown in Fig. 16 the plugging ECRH is responsible for the reduction in ion end losses. Once the barrier ECRH creates the hot mirror-confined electrons it can be turned off, since the hot electrons are long lived.

A feature of end plugging in TMX-U is that once the plugging ECRH power is off, the end losses rise very rapidly, in less than 1 ms. This is more rapidly than the plug or central cell densities change and, we believe, is due to the fact that the plugging potential is supported by the non-Maxwellian electron distribution function. The potential can therefore decrease on the electron relaxation time scale. In contrast, in TMX the end losses rise more slowly, on the 3- to 5-ms time scale required for the end plug ion density to decay. This provides further evidence that TMX-U end plugging occurs by thermal barrier type ECRH potential enhancement rather than by conventional tandem mirror plugging.

These experiments were operated with only one end plug. Consequently we could determine the end plug and central cell potential with end loss analyzers on each end wall. These measurements, shown in Fig. 17, indicate that during strong plugging, confining potentials of 0.6 kV are generated. This is twice the best achieved in our previous TMX experiments. We have not yet measured whether a thermal barrier dip in potential exists.

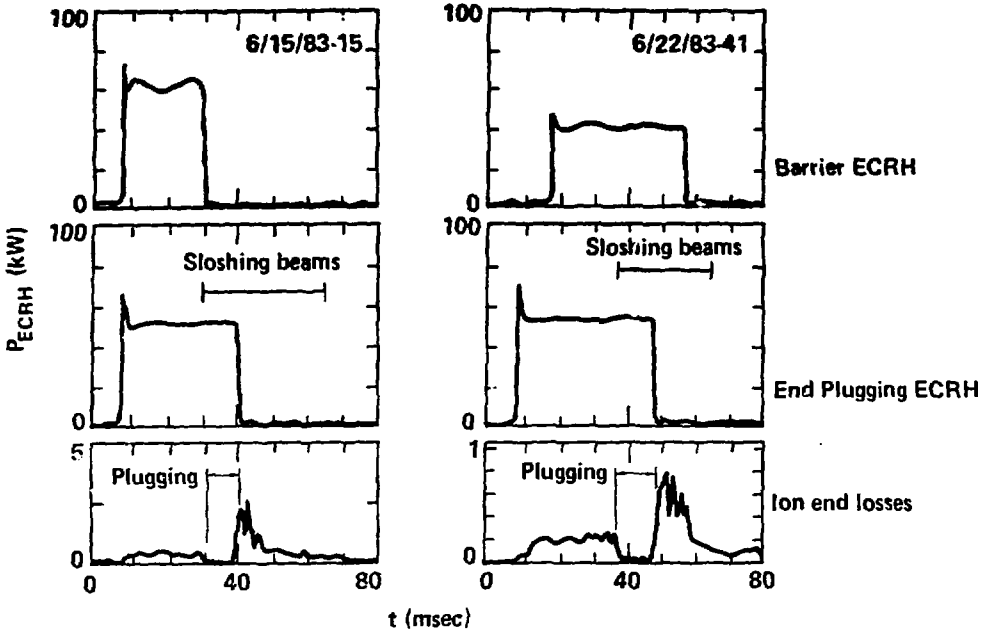

Figure 16. End plugging requires ECRH power at the potential peak. Shown vs time is (a) the barrier ECRH power, (b) the end plugging ECRH power and (c) the ion end loss current.

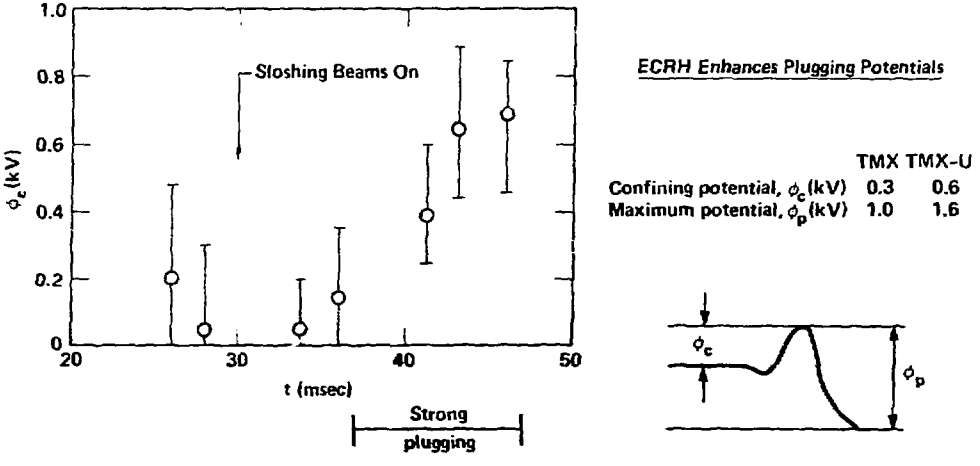

Figure 17. Measurements of plasma potential difference between west end plug and central cell. During strong end plugging a 0.4- to 0.7-kV confining potential is measured.

In addition to single-ended end plugging we have also plugged up both ends, as shown in Fig. 18. In this case both ends were plugged for 20 ms, the period of time when both ECRH and sloshing beams were on. In these early experiments we were learning how to increase the central cell density by central cell gas puffing. Consequently the temporal behavior of the density was quite irregular. In the data shown here the central cell and plug densities are nearly equal. In other experiments we have obtained plugging with $n_c = 2\ n_p$. This is the first time that we have observed electrostatic confinement without having the end plug density above the central cell density. As mentioned in the introduction, this is one of the distinguishing features of the thermal barrier concept.

When the ion end losses are so strongly reduced the ion end loss analyzer signal is mainly caused by electrons with energy sufficient to penetrate the 5-kV repeller. Consequently we can only estimate the axial confinement time to be 20 to 80 ms. At this time radial losses are most important. The radial confinement time determined from net current collectors is 4 to 8 ms. Radial losses always dominate the edge region. Radial loss in the core only dominates with strong axial plugging.

Absolutely essential to the success of these experiments is the control of cold gas from neutral-beam injectors and wall reflux. Figure 19 shows the pressure measured by an ionization gauge in the west end plug and west end fan tank together with the ion end loss current density. First note that the end plug pressure maintains below 10^{-6} Torr during the discharge. In operation without adequate titanium gettering on the walls the pressure continued to rise and ultimately terminated the end plugging. The time history of pressure in the end fan tank gives further evidence for strong end plugging. The pressure buildup ceases when the end losses are terminated. This very global measurement indicates that the end plugging is occurring across the entire plasma radius and that the reduction in ion end losses is not an instrumental effect, such as that caused by hot electrons penetrating into the end wall diagnostic instruments.

A remarkable feature of these end plugging experiments is that even with a plasma potential of 1.6 kV potential and without end losses to supply warm stabilizing ions, we did not observe any ion cyclotron fluctuations in the end cells. One explanation is that at the low densities of these experiments, $n_p = 3 \times 10^{11}$ cm^{-3} and the parallel wavelengths are long ($\lambda_{\parallel} \sim 3$ m) compared to the localized instability drive region. This region lies between the potential peak (peak of the sloshing-ion density) and the outboard mirror point where ion cyclotron fluctuations have previously been observed during high density sloshing-ion experiments. Whether fluctuations develop at full density (5×10^{12} cm^{-3}) and whether they remain benign, as in the sloshing-ion experiments described in Section IV, is one of the central issues to be resolved in future TMX-U experiments.

IV. Summary

Early TMX-U experiments at low density have shown very encouraging results. Sloshing-ion and hot-electron experiments have shown remarkable microstability and follow Fokker-Planck predictions. Potential enhancement driven by ECRH has been demonstrated and shown to produce strong end plugging with radial losses dominating. The facts that end plugging requires both ECRH and sloshing ions, and that end plugging can be generated with central cell densities exceeding end plug densities, strongly supports the thermal barrier concept. However, no direct measurements are yet available to determine if a

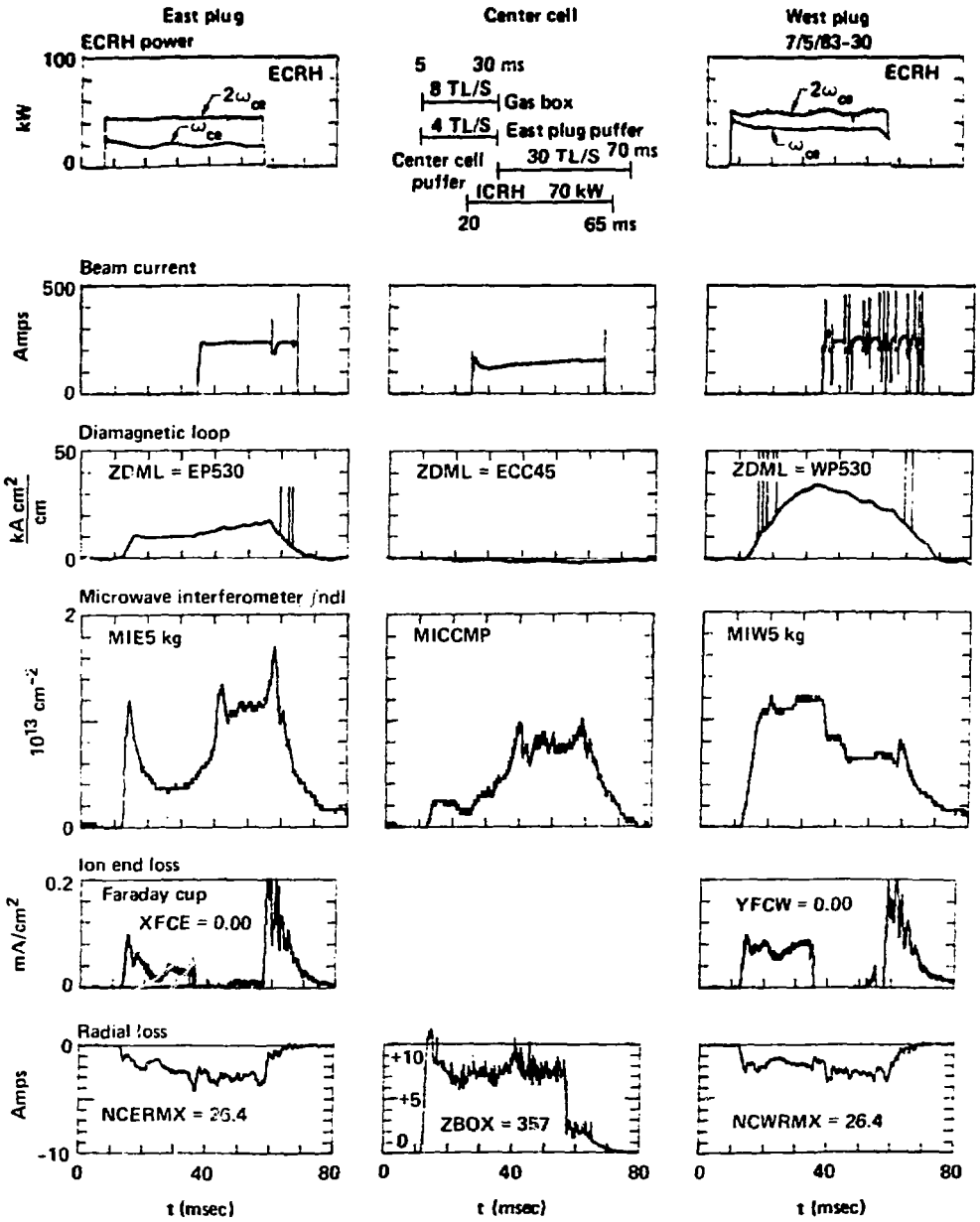

Figure 18. Measurements of end plugging on both ends. End plugging is limited by gyrotron pulse length. Shown are signals vs time in the east plug, central cell, and, west plug: (a) ECRH power, (b) beam power supply current, (c) diamagnetic loop, (d) microwave interferometer electron line density, (e) Faraday cup end loss current, and (f) radial loss current.

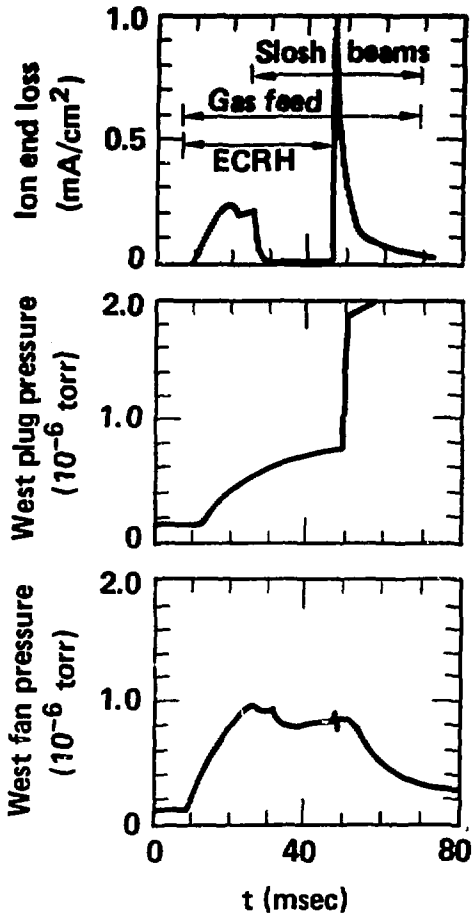

Figure 19. Measurements vs time of (a) the ion end losses, (b) plug region gas pressure and (c) end fan gas pressure.

thermal barrier potential dip is generated. Subsequent experiments will progress to higher densities with central cell ICRH, with an increased efficiency ECRH waveguide system, and with an improved gas feed system.

Acknowledgments

It is a pleasure to thank the many people who contributed to the work described in this report: the engineering groups, technical operations teams, computer group, theoretical and experimental physics groups, and the Sandia Laboratory surface interaction group.

This work was performed under the auspices of the U.S. Department of Energy by the Lawrence Livermore National Laboratory under contract number W-7405-ENG-48.

References

[1] F. H. Coensgen, T. C. Simonen, A. K. Chargin, and B. G. Logan, TMX-Upgrade Major Project Proposal, Lawrence Livermore National Laboratory, Livermore, CA, LLL-Prop-172 (April 1980).

[2] D. E. Baldwin and B. G. Logan, "Improved Tandem Mirror Fusion Reactors", Phys. Rev. Lett. 43, 1318 (1979).

[3] D. L. Correll, S. L. Allen, and T. A. Casper et al., "Ambipolar Potential Formation and Axial Confinement in TMX," Nucl. Fusion 22, 223 (1982).

[4] S. L. Allen, T. A. Casper, J. F. Clauser et al., Summary of Results from the Tandem Mirror Experiment (TMX), Lawrence Livermore National Laboratory, Livermore, CA, UCRL-53120 (1981).

[5] T. C. Simonen, "Experimental Progress in Magnetic-Mirror Fusion Research," Proc. IEEE, 1981 (IEEE, Piscataway, NJ, 1981) 69, 935-957 (1981).

[6] T. K. Fowler and B. G. Logan, "Tandem Mirror Reactor," Comments Plasma Phys. Controlled Fusion 2, 167 (1977).

[7] G. I. Dimov, V. V. Zahaidahov, and M. E. Kishinevshii, "Thermonuclear Confinement System with Two Mirror Systems," Fiz. Plasmy 2, 597 (1976); [Sov. J. Plasma Phys. 2, 326 (1976)].

[8] G. A. Carlson, B. Arfin, and W. L. Barr et al., Tandem Mirror Reactor with Thermal Barriers, Lawrence Livermore National Laboratory, Livermore, CA, UCRL-52836 (1979).

[9] T. A. Casper and G. R. Smith, "Observation of Alfven Ion Cyclotron Fluctuations in the End-Cell Plasma in the Tandem Mirror Experiment," Phys. Rev. Letters, 48, 1015 (1982).

[10] R. H. Cohen, Potentials in Thermal Barriers with Strong Electron Cyclotron Heating, Lawrence Livermore National Laboratory, Livermore, CA, UCRL-88939 (1983) (to be published in Phys. Fluids Lett.).

[11] Y. Matsuda and T. Rognlien, Numerical Solution of the Electron Distribution Function in Tandem-Mirror Thermal Barriers, Lawrence Livermore National Laboratory, Livermore, CA, UCRL-89124 (1983).

[12] A. W. Molvik and S. Falabella, Use of ICRH for Startup and Initial Heating of the TMX-U Central Cell, Lawrence Livermore National Laboratory, Livermore, CA, UCID-19342 (1982).

[13] B. W. Stallard, "Experiments on Hot-Electron ECRH in the Tandem Mirror Experiment-Upgrade," in 5th Topical Conference on RF Plasma Heating, Madison, Wisconsin, 1983 (University of Wisconsin, Madison, WI, 1983).

[14] Y. J. Chen, W. M. Nevins, and G. R. Smith, "High Frequency Microinstabilities in Hot-Electron Plasmas," Proceedings of the 2nd Workshop on Hot Electron Ring Physics, 1981, (Oak Ridge National Laboratory, Oak Ridge, TN, 1981), Vol 1, p. 279.

[15] M. Porkolab, Upper Hybrid Loss-Cone Instability in Tandem Mirror Thermal Barriers," Lawrence Livermore National Laboratory, Livermore, CA, UCRL-89033 (1983) (to be published in Phys. Fluids).

[16] T. A. Casper, Y. J. Chen, R. Ellis, R. James, and C. Lasnier, Assessment of Hot Electron Microstability in the Initial TMX-U Experiments, Lawrence Livermore National Laboratory, Livermore, CA, UCID-19783 (1983).

[17] T. C. Simonen, S. L. Allen, and T. A. Casper, "Operation of the Tandem-Mirror Plasma Experiment with Skew Neutral-Beam Injection," Phys. Rev. Letters 50, 1668 (1983).

[18] T. J. Orzechowski, S. L. Allen, J. H. Foote et al., Measurements of Sloshing Ion Spatial Projects in End Cell of Tandem Mirror Experiment-Upgrade (TMX-U), Lawrence Livermore National Laboratory, Livermore, CA, UCRL-88447 (1983).